J. COMBIN. MATH. COMBIN. COMPUT. 127b (2025) 893--909

Journal of Combinatorial Mathematics and Combinatorial Computing
www.combinatorialpress.com/jcmcc

Combinatorial Press

Application and Algorithm Design of Multi-Channel Sensor Fusion Technology for Laser Spot Detection

Keya Yuan[1], Lin Li[2,✉]

[1] College of Robotics, Beijing Union University, Beijing, 100101, China
[2] College of Applied Science and Technology, Beijing Union University, Beijing, 100101, China

ABSTRACT
According to the principle, characteristics and use of CCD, this paper designs a laser beam quality measurement program using CCD as a beacon light capture detector and proposes a laser spot detection method based on CCD. The experimental steps and calculation steps for laser beam width measurement and laser power measurement by CCD camera are proposed respectively. The beacon light is used as a light source, and the spot image is processed according to the principle of gray-scale image thresholding to capture the beacon light and present it in the form of a spot on the CCD image sensor. Then, through binarization processing, the spot of the beacon light is distinguished from the background, so as to realize the spot position detection of the beacon light beam. The image data are collected to experimentally detect the laser spot position detection algorithm based on CCD image sensor proposed in this paper, respectively. In the fine-tracking spot position detection, the spot is adjusted in the range of ±9.25mrad, and the solution value 1_{min} is set to be determined every 0.78mrad. The spot center is kept in the range of ±9.05mrad, and centering is carried out every 0.003mrad according to the fine-centering algorithm. The experimental results show that the spots after fine centering are all within the range of ±0.78mrad, and the change trend is consistent with the simulation results, so the laser spot position detection algorithm proposed in this paper is feasible in fine tracking spot position detection.

Keywords: beamwidth measurement, binarization, spot detection, CCD sensor, beacon light

1. Introduction

Lasers are another important new technology that has developed rapidly in this century, following atomic energy and semiconductors. The development of laser types and quality is still on the rise. With the increasing maturity of laser technology, lasers have been widely used in the fields of communication, military, aerospace, and medicine [1-4]. In practical applications, the measurement of

✉ Corresponding author.
E-mail address: lilin_buu@163.com (L. Li).
Received 05 January 2024; Revised 15 April 2024; Accepted 05 October 2024; Published Online 16 April 2025.
DOI: 10.61091/jcmcc127b-050

laser parameters is a basic work of laser technology, but also an important aspect, in which the fast and accurate detection of laser spot is one of the key links. The detection of laser spot is mainly applied to two aspects. On the one hand, by detecting the position of the laser spot for high-precision displacement measurement. The main idea of this technology is that when the target to be detected moves, the spot captured by the detector will also change, and the change of the spot center coordinates is calculated by algorithm to evaluate the displacement, which is widely used in laser manufacturing, bridge, tunneling and other fields [5-7]. On the other hand, by detecting whether there is a laser spot in the field or tracking the spot for off-target uploading, the technology is mainly used in laser warning, laser guidance and other military fields [8-10]. Whether it is for displacement measurement or tracking the spot, first of all, we need to use a good method to detect the spot and calculate its center coordinates.

Multi-channel sensor fusion is a technology that utilizes information from two or more sensors and processes the data through fusion algorithms to improve the sensors' performance, accuracy and robustness to the environment [11-12]. This technology can obtain more accurate data through the comprehensive analysis of multiple information measured, which is of great significance for automation control, machine generation, intelligent transportation, security monitoring and other application areas [13-16]. Generally speaking, multi-channel sensor fusion technology includes three aspects: information fusion, data fusion and feature fusion [17-19]. Among them, information fusion combines sensor information according to a certain law to obtain new information; data fusion is to fuse the raw data collected by sensors to obtain more accurate data, thus improving the accuracy of environmental perception; and feature fusion combines feature information extracted from different sensors to obtain more detailed and complex feature information, thus improving the ability to analyze the environment. The feature fusion is to merge the feature information extracted from different sensors to obtain more detailed and complex feature information, thus improving the analyzing ability of the environment.

At present, the detection of laser spot has become a research field of great concern, and its detection accuracy has a significant impact on the improvement of lasers, laser diagnosis and medical treatment, and monitoring of special targets. There have been collaborative applications in multi-channel sensor fusion with lasers [20-22].

This paper analyzes the working principle of CCD image sensor, assembles laser parameters and CCD characteristic parameters, and designs a laser beam quality measurement scheme (including beam beamwidth measurement and laser power measurement) to prepare for the subsequent laser spot detection experiments. The CCD is used as the beacon light capture detector, and the gray-scale image thresholding is used to separate the background region from the target region. The threshold value is obtained from the “valley” and “peak” elements in the grayscale histogram. The threshold value is binarized to obtain the spatial information of the beacon light and the spot position. Set the experimental parameters of laser beam detection, and carry out fine-tracking spot position detection and coarse-tracking spot position detection respectively.

2. Laser spot detection program design

2.1. Laser parameters

The fundamental properties of laser beams are of great importance for the development of laser optics as well as for the measurement of laser beam parameters.

Among the forms of laser beams, the fundamental mode is the most important and typical one.

Different resonant cavity structures have different mode structures and mode-limiting properties, and the frequencies and directions that may occur in a resonant cavity are called eigenmodes. Transverse and longitudinal modes are distinguished by direction and frequency, but they are not mutually exclusive. Typically, TEM_{mn} is used to characterize the laser light field propagating in the direction of the laser's optical axis, where m and n denote the number of wave segments perpendicular to the beam cross-section and perpendicular to the direction of propagation, respectively. TEM_{00} is called the fundamental mode, also called the single-phase mode, which has the widest range of applications. The energy distribution of the fundamental mode laser beam is highly concentrated, and the center of curvature changes with the propagation process. Within the cross-section along the laser propagation direction, the luminous flux density exhibits an ideal Gaussian distribution shape. Therefore, the fundamental mode laser beam is also called a Gaussian beam.

As an example, a Gaussian beam output in a stable resonant cavity and a homogeneous medium is explored in the TEM_{00}th lowest order transverse mode.

All optical fields follow Maxwell's system of equations, so the mode field of the stabilized resonant cavity should also be a solution of this system of equations. Setting the z-axis as the propagation direction of the laser beam, the Gaussian beam can be expressed as follows:

$$\begin{gathered} E(x,y,z) = A(x,y,z)\exp[\psi(x,y,z)] \\ A(x,y,z) = E_0\frac{\omega_0}{\omega(z)}\exp\left[-\frac{r^2}{\omega^2(z)}\right] \\ \psi(x,y,z) = -ik\left[z + i\varphi(z) + \frac{r^2}{2R(z)}\right] \\ r^2 = x^2 + y^2 + z^2 \end{gathered} \tag{1}$$

where the beam parameters are introduced:

$$\begin{cases} \omega^2(z) = \omega_0^2\left[1+\dfrac{z^2}{z_0^2}\right] \\ R(z) = z\left[1+\dfrac{z_0^2}{z^2}\right] \\ \varphi(z) = \tan^{-1}\left(\dfrac{z}{z_0}\right) \\ z_0 = \dfrac{\pi\omega_0^2 n}{\lambda} \end{cases} \tag{2}$$

In Eq. (2), $A(x,y,z)$ denotes the amplitude term and $\psi(x,y,z)$ denotes the phase term. The formula represents a solution of the fluctuation equation in a homogeneous medium, called the fundamental Gaussian beam solution. The transverse properties of this solution are only related to the spatial position.

The purpose of this section is to describe the laser parameters, including beam beamwidth, beam waist position, beam scattering angle, and laser beam quality M^2 factor, which will help in the subsequent laser parameter detection.

Beamwidth, also known as beam diameter, is the diameter of the beam cross-section perpendicular to the z-axis when the laser beam is traveling along the z-axis. Since the laser spot has the highest intensity in the center and decreases in intensity along the perimeter, there is no clear edge to characterize the spot size. Therefore, the beam width can be defined in a number of ways. Commonly used, including the definition of the full width of the half-peak, the definition of the second-order moments.

Beam dispersion angle: Define the z-axis as the direction of propagation of the laser beam, then the far-field dispersion angle θ is defined as:

$$\theta = \lim_{x \to \infty} \frac{\omega(z)}{z} \tag{3}$$

In equation (3), $\omega(z)$ is the beamwidth.

When performing practical measurements, the position of the laser's beam waist is inconvenient to measure directly and is usually located in the cavity or in the front section of the laser. Therefore, a phase-independent optical system is usually used to adjust the position of the artificial laser beam waist to make it easy to observe. A plano-convex lens is usually chosen to converge the laser and the far-field divergence angle of the artificial beam waist is measured.

The laser beam quality M^2 factor is defined as:

$$M^2 = \frac{\omega\theta}{\omega_0\theta_0} \tag{4}$$

In Equation (4), ω is the beamwidth of the measured laser beam, and θ is the far-field divergence angle of the measured laser beam. ω_0 represents the beamwidth of the ideal laser beam, and θ_0 represents the far-field divergence angle of the ideal laser beam. The M^2 factor takes into account both the effect of changes in the near field (beam waist width) on the quality of the laser beam and the effect of the far field (divergence angle). When the laser beam passes through an ideal diffraction-free, aberration-free optical system, the M^2 factor is an invariant, which avoids the uncertainty associated with evaluating the beam quality using only the focused spot size or the far-field divergence angle.

2.2. CCD Image Sensor

CCD is called charge-coupled device, also called image sensor [23]. It is a semiconductor device that converts optical signals into electrical signals, and in the design of various CCDs, there must be a CCD driver circuit.

2.2.1. Principle of CCD operation. CCD image sensor working principle, can be divided into four steps:

1) Photoelectric conversion (optical signal is converted to signal charge). Photoelectric conversion is the existence of electrons in the material due to light after the energy, then only need to apply a small electric field, the electrons can produce a free movement of the state. This means that a signal charge is generated according to the intensity of light irradiated onto the light-sensitive surface, and the signal charge generated is proportional to the intensity of light irradiation. From a physical point of view, the action can be divided into two cases. One is the internal photoelectric effect, in which electrons within a solid can be divided into several energy levels according to the energy they possess. The lower energy electrons in the energy levels are excited into higher energy electrons due to the energy of the photons. The other is the external photoelectric effect, where electrons absorbing the energy of photons on the surface of a solid are excited into a vacuum. And the CCD image sensor utilizes the internal photoelectric effect to complete the photoelectric conversion.

In the CCD image sensor, there are two energy levels of electrons, valence band and conduction band. When the valence band of electrons absorbed into the photon energy is released to the conduction band, at this time, only need to apply a small voltage to the substrate, the electrons will be able to move, so according to the strength of the light will be able to get the corresponding signal charge.

2) Charge storage (storage of signal charge). Charge storage is the action of storing the signal charge obtained after photoelectric conversion. However, CCD photoelectric conversion after the signal charge can not be stored in the potential well for a long time, but only temporary storage of the signal charge.

3) Charge transfer (transfer signal charge). Can be summarized in one sentence to the CCD charge transfer principle, that is, to move the signal charge stored in the potential well.

4) Charge detection (signal charge is converted to a voltage signal and then output). Charge detection is the transfer over the charge signal is converted to an electrical signal, that is, the transfer over the signal charge is converted to a change in the voltage at the ends of the capacitor.

2.2.2. CCD Characterization Parameters:

1) Sensitivity: sensitivity indicates the image acquisition environment in what degree of darkness, the CCD can capture images.

Several important factors affecting sensitivity are as follows:

(1) Quantum efficiency of the photodiode.

(2) Micro lens.

(3) The conversion efficiency of the FD.

2) Dynamic range: It is defined as the ratio of the maximum amount of signal stored in the potential well to the minimum amount of signal from noise.

3) Resolution: Simply put, resolution refers to the degree of clarity presented by the image captured by the CCD. The greater the number of pixels of the CCD, the clearer the image presented, so the higher the resolution proved. Therefore, often use the number of CCD pixels to replace the resolution.

4) Sensitivity: it is one of the important parameters of the CCD. It has two meanings, one meaning is that it represents the ability of the CCD to complete the photoelectric conversion. Another meaning is that the CCD sensor can sense the minimum illumination, the unit is lux (lx) or watt (W).

2.3. Laser beam quality measurement program design

2.3.1. CCD Camera-Based Beamwidth Measurement

1) CCD camera-based beamwidth measurement scheme. In this paper, we use the CCD camera-based beamwidth measurement scheme, which uses hardware including a laser with a wavelength of 532 nm and a power of 50 m W, an attenuator set, a phase-independent lens, a Hikvision grayscale camera, a sliding platform and a computer.

2) Experimental steps for beamwidth measurement. Adjust the position of the laser and CCD camera before the start of the experiment. First of all, make the optical axis center and CCD camera lens center in the same horizontal axis. Place the attenuator so that the laser beam through the attenuator attenuation of optical power, placed without aberration lens to focus the beam to form a simulated beam waist. Then slide the platform along the direction of the optical axis, so that the camera in the simulation of the beam waist near the left and right movement, in order to capture different positions at the spot image.

The beamwidth size at each position was calculated, and finally the spot transverse diameter $\omega_x(z)$ and spot longitudinal diameter $\omega_y(z)$ data at different positions were recorded by computer. Fit the Gaussian laser beam hyperbolic model according to the least squares method.

3) Beamwidth Calculation Steps. In practice, the acquired spot data, after image denoising, will still have a small amount of noise. Due to the effect of noise so that all the beamwidth points obtained does not enclose an ideal circle, but fluctuates around the circle.

If only select a picture of the marker points to calculate the beamwidth size will produce errors, so this paper uses the average value of the beamwidth size, the method can reduce the noise-induced errors, the specific steps of the algorithm are as follows:

Step1: Iterate through all the pixel points on the denoised light spot image, find out all the points whose gray value is $1/e^2$ times of the maximum gray value (the brightest point), and mark these points as red.

Step2: Calculate the horizontal and vertical distance between the center of mass of the spot and each marked point.

Step3: Add up the distances and take the average value, and this horizontal and vertical average value is regarded as the width of the spot.

Step4: At the same position, take 10 pictures, use Step1 to Step3 to calculate the beam width value of 10 pictures, and take the average value as the beam width value of this position.

2.3.2. Measuring laser power based on CCD camera:

1) CCD Camera Laser Power Measurement Experiment. In this chapter, the CCD camera measurement of laser power experiment is designed to verify the feasibility of using a CCD camera and diffuse reflective plate instead of the function of the surface array detector.CCD camera measurement of laser power system consists of the wavelength of 532nm, power 50m W laser, attenuator group, Hikvision grayscale camera, optical power meter, diffuse reflective plate and the computer components.

2) CCD camera measurement of laser power experiment steps. Fix the position of the laser and the CCD camera so that the angle between the laser and the CCD camera is as small as possible θ. An increase in θ will cause distortion of the spot image captured by the CCD camera. Adjust the focal length of the CCD camera so that the diffuse reflector plate is completely in the field of view of the camera, and align the CCD camera with the center of the diffuse reflector plate. Place the attenuator in front of the emitting end of the laser, and adjust the attenuation degree of the attenuator so that the maximum gray value of the spot image captured by the CCD camera is around 230. A 5mm round hole is made in the center of the diffuse reflecting plate, and an optical power meter is placed behind the hole to monitor the laser power through the aperture. Combined with the gray scale distribution of the spot image, the total spot power is calculated.

3) Calculation steps for laser power measurement by CCD camera. After the laser beam is irradiated to the diffuse reflector plate, it is known from the diffuse reflector plate characteristics that the reflected light intensity is equal in all directions. Therefore, regions with equal gray values within the laser spot have the same energy distribution law. The power level displayed by this optical power meter is recorded at the same time as the spot image is acquired. Assuming that the power of the laser beam through the circular hole measured by the power meter is xmW, the power magnitude corresponding to the unit gray value is calculated, and thus the power magnitude of the entire spot is calculated.

The aperture on the diffuse reflecting plate is a circle, assuming that the diameter of the circle is r pixel lengths, and a square with side length r, the intersection of the diagonals of the square coincides with the center of the circle, then the number of pixels accounted for by the square is r^2. Theoretically, the number of pixels accounted for by the circle is $\pi x^2 / 4$. The total power of the spot is calculated as follows, assuming that the total gray value of pixels in the square is y_x, and the total gray value of the spot is sum:

The total gray value inside the circular hole y_r is:

$$y_r = \pi y_s / 4 \tag{5}$$

The total power in the square is:

$$k = 4x / \pi \tag{6}$$

Then the power corresponding to the unit gray value is:

$$e_0 = 4x / \pi y_s \tag{7}$$

The total power of the spot image is:

$$E = sum \times e_0 \tag{8}$$

2.4. CCD-based laser spot detection method

2.4.1. Beacon Light Capture Determination. Beacon light, as a light source, should have a higher average gray level than the background light. According to the principle of gray-scale image thresholding, if a suitable gray level is selected as the threshold, the pixels below the threshold indicate the background, and the pixels above the threshold indicate the beacon light.

The specific beacon light capturing decision process is as follows:

Let the captured gray-scale image be $I(x, y)$, determine a threshold T by the algorithm, and threshold $I(x, y)$ to get:

$$G(x,y) = \begin{cases} g_{high} & I(x,y) \geq T \\ g_{low} & I(x,y) < T \end{cases} T \in [0, L-1] \tag{9}$$

The number of pixels in image $I(x, y)$ that satisfy g_{high} is then counted and obtained:

$$n = \sum_{x,y \in D} P_{xy} P_{xy} \geq T \tag{10}$$

Take the number of normalized pixels:

$$C = \frac{S}{N} \tag{11}$$

In Eq. (11) S is the spot size. N is the total number of pixels in the image, and it is easy to know $n \leq N$ and $0 \leq C \leq 1$.

So the judgment condition of capture depends on the threshold value T and the corresponding normalized pixel number C. How to determine whether the beacon light is captured is shown in Eq. (12):

$$\begin{cases} \text{Success } n / N \geq C \\ \text{Failure } n / N < C \end{cases} \tag{12}$$

For the normalized pixel number C, as it relates to the size of the spot, it can generally be chosen flexibly for different environmental conditions by means of measured empirical values, and the key lies in the selection of the threshold value T.

2.4.2. Algorithm for obtaining thresholds. Looking at the "peaks" in the grayscale histogram, we can see that the "peaks" should have a certain height in the first place, and the heights within a certain width around the "peaks" are lower than the height of the "peaks" [24]. If you define an integer array zhiFANG, the value of the zhiFANG element in the array is equal to the number of pixels in the grayscale graph with a grayscale value equal to i. The above two features correspond to the fact that the value of the element in the array corresponding to the "peak" should be greater than a given value of H. And the values of a certain number of elements around it are less than it.

The "valley" in the grayscale histogram should correspond to the element with the smallest value between the two "peak" elements in the array, and the grayscale value corresponding to that element is the T to be obtained. According to the above description, the procedure flow for obtaining the threshold is shown in Figure 1.

In the figure, H is the variable representing the height of the peak, and kuan is the variable representing the minimum width of the peak. The variables fengZhiS and fengZhiS are used to store the grayscale values where the two peaks are located.

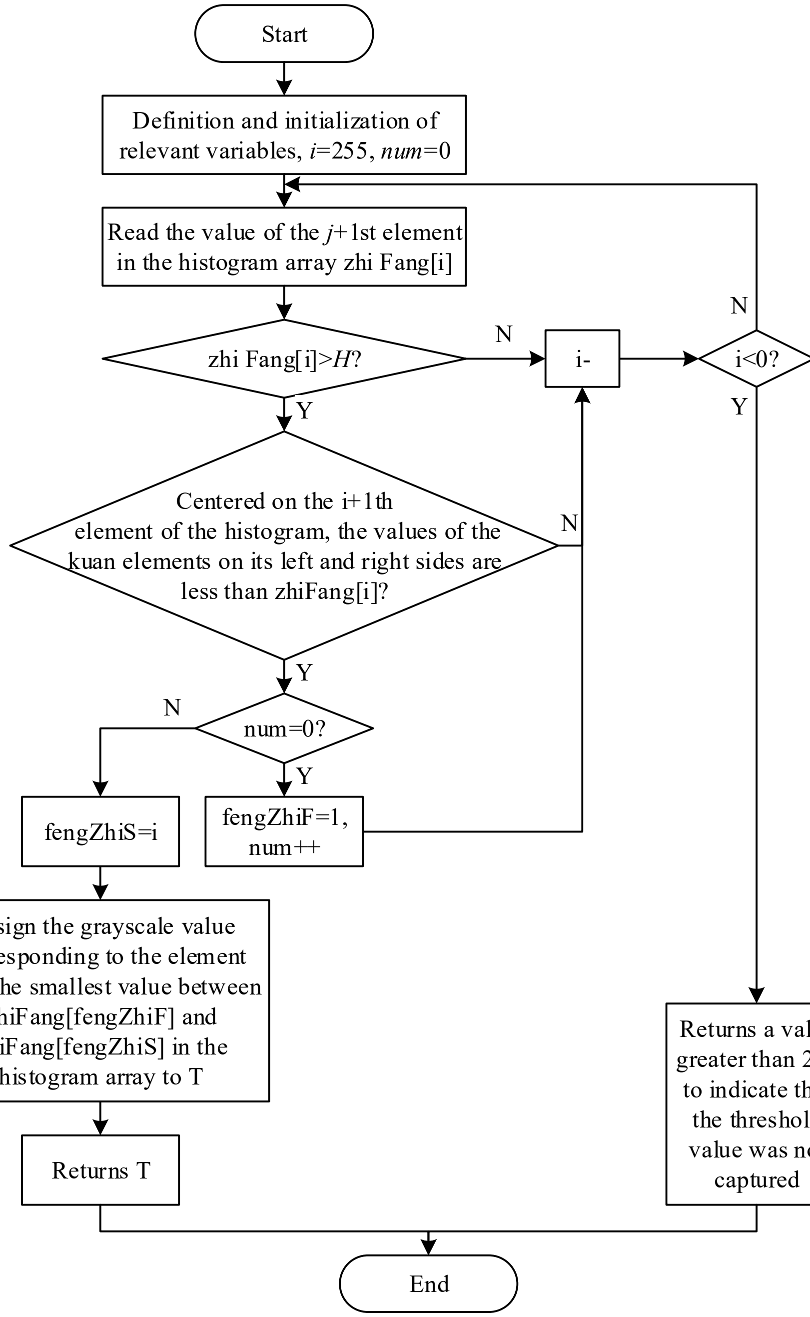

Fig. 1. Process of obtaining the valve value

2.4.3. Beacon light spot image extraction. The captured beacon light forms a spot on the CCD, and that part is the beacon light portion of the image. The spot image extraction of the beacon light is to separate the spot part of the whole image. Through the previous analysis, it is known that using the grayscale histogram to represent the image does not obtain the spatial information of the image, and it is necessary to find other representation methods. One of the most important conditions for capture determination is the boundary threshold T. By T the gray scale histogram is distinguished into two parts, the beacon light and the background, so the boundary threshold can be applied to the image and the image can be binarized to get the spatial information of the beacon light [25].

According to equation (13), the binarized image is obtained if $g_{high} = 1$, $g_{low} = 0$ are taken:

$$B(x,y)=\begin{cases}1 & I(x,y)\ge T\\ 0 & I(x,y)<T\end{cases} T\in[0,L-1] \tag{13}$$

After binarization, the spot of the beacon light can be clearly distinguished from the background from the image.

The selection of the threshold value determines the size of the spot after binarization, and according to the maximum variance criterion, the optimal queue value should maximize the total variance of the spot (target) and the background. By dividing the image into two regions, spot S and background B, with threshold T, the probability of gray level occurrence is respectively:

$$P_B=\sum_{i=0}^{T-1}P_i=\sum_{l=0}^{T-1}\frac{N_i}{N}\equiv P(T) \tag{14}$$

$$P_S\equiv 1-P(T) \tag{15}$$

The average gray scale is respectively:

$$\mu_B=\frac{1}{P_B}\sum_{i=0}^{T-1}iP_i\equiv\frac{\mu(T)}{P(T)} \tag{16}$$

$$\mu_S\equiv\frac{\bar{\mu}-\mu(T)}{1-P(T)} \tag{17}$$

where $\bar{\mu}$ is the average gray level of the whole graph, the total variance is:

$$\begin{aligned}\bar{\sigma}^2(T)&=P_S\left(\mu_s-\bar{\mu}\right)^2+P_B\left(\mu_B-\bar{\mu}\right)^2\\&=\frac{[\bar{\mu}P(T)-\mu(T)]^2}{P(T)[1-P(T)]}\end{aligned} \tag{18}$$

Binarization of the image by appropriate thresholding is mainly to simplify the post-processing work. While preserving the original image, only the copied image is binarized, and finally the binarized image is multiplied with the original image, so that only the image containing the spot information will be obtained, and the value of pixels other than the spot will be 0. Operations such as median filtering on this image will be much more efficient than that on the original image, which will greatly save time.

2.4.4. Center of gravity extraction algorithm for light spots. Through the position of the center of gravity of the incident spot of the beacon light in the CCD image, the current position relationship between the transmitter and receiver of the beacon light can be learned. To provide a basis for the antenna orientation adjustment, so in the selection of the algorithm to try to make the calculation results accurate and reliable.

The center of gravity algorithm has high accuracy, good stability, fast calculation and processing, and is an effective algorithm for spot position extraction and localization in beacon light capture technology.

The center of gravity algorithm is based on the principle of seeking the center of gravity in plane geometry.CCD is an array image sensor device with pixel as unit. When using a CCD to determine the position of the spot imaged on the CCD image plane, it is important to consider that the spot is not a geometric point, and the distribution of spot light intensity is often close to a Gaussian distribution. If a spot consists of m pixel, each pixel corresponds to a defined spatial coordinate (x,y) and a gray value $G(x,y)$, then the center of gravity of the spot is:

$$\begin{cases} X = \dfrac{\sum_{i=1}^{m} x_i G_i(x_i, y_i)}{\sum_{i=1}^{m} G_i(x_i, y_i)} \\ Y = \dfrac{\sum_{i=1}^{m} y_i G_i(x_i, y_i)}{\sum_{i=1}^{m} G_i(x_i, y_i)} \end{cases} \tag{19}$$

In Eq. (19) $G_i(x_i, y_i) = s_i + n_i$ is the gray value of the ind pixel point, s_i and n_i are the original image gray value and image noise respectively. x_i and y_i are the coordinates of the pixel point in the image in pixels, respectively.

From the previous conditions for the establishment of the formula, it can be seen that in order to use Eq. (19) to directly extract the center of gravity of the spot on the original image captured by the CCD for spot extraction, it is necessary to first obtain the coordinates of all the pixel points occupied by the spot in the image and store them first. By using Eq. (19) and combining it with the binarization method, the extraction of the center of gravity of the spot can be easily achieved.

3. Experimental preparation for laser spot detection

In this paper, according to the design principle of CCD image sensor, we design the structure of laser spot detection system and write relevant software and hardware processing programs to realize spot center detection. The design focuses on three modules of image acquisition, storage and processing. In order to verify the correctness of the system function, the system image acquisition and processing process is verified on the PCB circuit board, and the experimental results are analyzed.

3.1. Image data acquisition and transmission experiment

The main equipments for the experiment are: laser light source, spot receiving screen, CMOS camera, PCB circuit board, USB upload module, standard dot matrix sample board for experiment and computer.

The laser light source sends out a laser beam at a certain distance, hitting the glass receiving screen pasted with sulfuric acid paper. By adjusting the thickness of the sulfate paper and the angle of the receiving screen, a circular spot with uniform illumination and shape can be obtained. The imaging role of the receiving screen is very important, if the laser beam directly irradiated to the CCD image sensor will cause brightness saturation and chip damage.

3.2. Configuration of experimental parameters

After the system is powered up, the FPGA performs I2C configuration of the CCD camera, including image pixel size and acquisition clock configuration.

The default size of the image sensor for this system is 2048*1024, and the maximum acquisition rate at this pixel is 13fps (frames per second). The image size can be changed by configuring the registers and deciding to output an image of any area on the entire photosensitive surface.

In this system, it is not necessary to acquire an image of size 2048*1024. The higher the image pixels, the lower the acquisition rate. The subsequent processing speed is also slower, which will greatly reduce the system real-time requirements. At the same time, the acquisition of large-area images is not easy to ensure the uniformity of light, which is easy to bring about system errors.

Through experiments, this paper will CCD output image is set to 512 * 512 size, in the complete acquisition of the target spot area under the premise of reducing the image pixels to facilitate subsequent processing.

The maximum output pixel clock frequency of the CCD sensor is 52MHz, which can be changed through the configuration register. Under 512*512 image size. The relationship between acquisition rate and output pixel clock is shown in Table 1.

It is found that the faster the image acquisition rate, the lower the image quality. Under the premise of ensuring the real-time nature of the system, the pixel clock of 6MHz is selected in this paper to obtain higher quality images.

Table 1. The relationship between the gathering rate and the output pixel clock

Pixel clock	52MHz	24 MHz	12 MHz	6 MHz
Frame rate	93FPS	54FPS	25FPS	13 FPS

4. Laser spot detection results and analysis

In this paper, the laser spot detection algorithm for CCD image sensor based laser spot detection is performed for fine tracking spot position detection and coarse tracking spot position detection respectively.

4.1. Validation of Precision Tracking Spot Position Detection Algorithm

Precision tracking servo unit is mainly composed of the following parts: precision tracking spot detection components, two-dimensional precision fast tilt galvanometer galvanometer, spot off-target volume processing unit.

The board components of the fine-tracking detection spot image processing unit include Cameralink interface, interface chip, FPGA main chip, SRAM, ADV7125, high-speed serial chip, power supply and VGA interface, composite video output interface.

The Cameralink interface receives digital spot image information and sends it to the FPGA through the interface chip to complete the level conversion; the FPGA processes the spot image to get the off-target amount and buffers the image to the off-chip RAM for the VGA controller to use. The off-target quantity is converted into differential signal by high-speed serial chip and sent to the next level servo unit, and the image to be displayed by VGA controller is sent to the external video D/A chip, which is converted into analog VGA signal or CVBS composite video signal, and then sent to monitor to display the spot image.

After the communication beam is suppressed by the coarse tracking servo system, its tracking residual is smaller than the fine tracking field of view. The coarse tracking residual sequence is shown in Fig. 2, which shows the off-target amount of the spot when the fine tracking system is not activated, and the amplitude of the coarse tracking residual sequence is controlled at [-45,35].

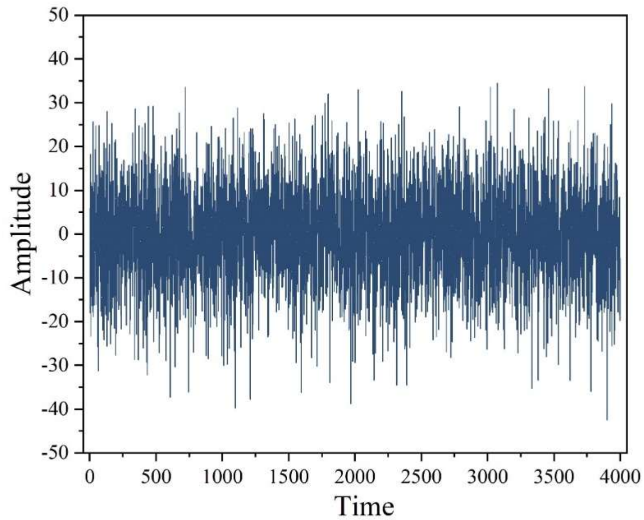

Fig. 2. Coarse trace suppression of the residues

After suppression by the coarse tracking servo system, the fine tracking servo system is turned on. The time-domain curves of the spot off-shift volume before and after the fine-tracking suppression are shown in Fig. 3, which shows that the off-target volume suppression effect is obvious, and the suppression of the residual sequence occurs after 3100s, and the residual sequence is kept at [-40,35].

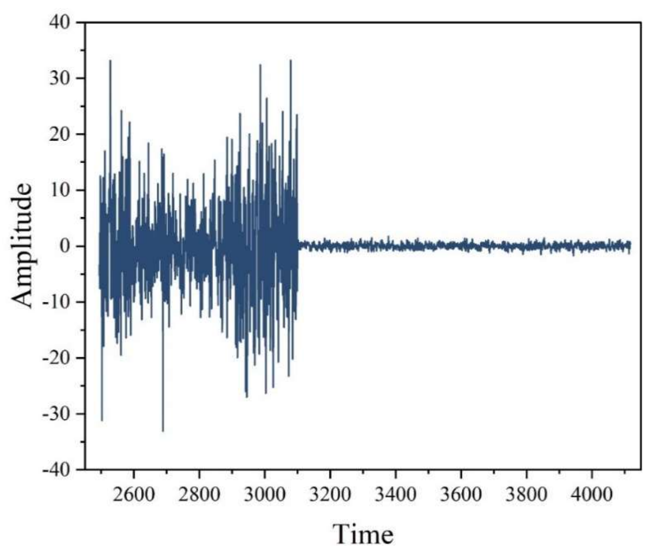

Fig. 3. The time domain curve of the spot removal class

The time-domain curve of the fine-tracking residuals and its histogram statistics are shown in Fig. 4, and the histogram shows that the fine-tracking residuals are mainly distributed in [-0.2,0.2], and the tracking accuracy $\pm 3\mu rad$ is realized according to the statistics.

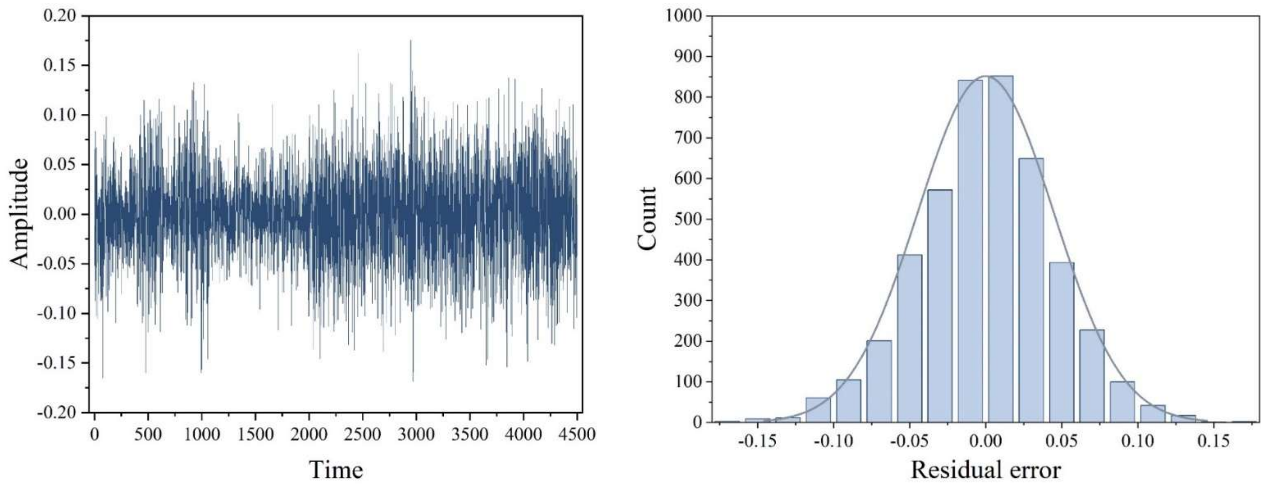

(a) Precision tracking domain residue (b) Statistical histogram of residual difference

Fig. 4. Precision trace residual difference time domain curve and histogram result

Spectral analysis of the data after fine-tracking suppression, the fine-tracking residual vibration power spectrum is shown in Fig. 5. It can be found that there are two peak regions, one is the 2~80Hz region. It is the low-frequency envelope of the fine-tracking suppressed residual corresponding to the fine-tracking residual. The other is 100~200Hz region. It is the fine tracking bandwidth matching corresponding to the high frequency random noise of the fine tracking residuals.

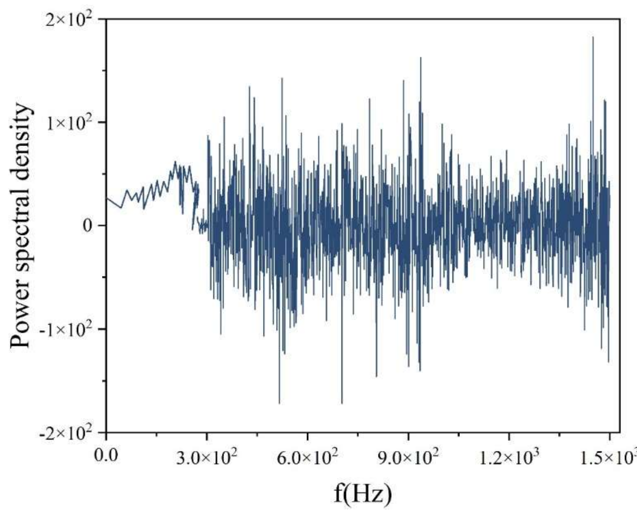

Fig. 5. Finishing track residual vibration power spectrum

4.2. Coarse tracking spot position detection algorithm validation

On a built-up coarse tracking test bed, the laser is controlled to output a laser beam of 30 μW . The laser beam is shaped by a parallel light pipe and adjusted to approximate a parallel beam. The beam is reflected by a fast deflector that controls the direction of the laser beam, and then focused behind a lens controlled by an electrically moved stage. The radius of the spot projected on the array detector is adjusted to r =3.74mm by controlling the focal length L_{max} of the lens behind the electrically moving platform.The array detector unit outputs photocurrent based on the photoelectric effect, which is converted into an analog voltage signal by the amplification circuit and the data acquisition circuit. The voltage signal is converted into a digital signal by the data acquisition system and transmitted to the multipoint control unit. The centering algorithm is used to calculate the centering step, and the signal is transmitted to the fast deflector mirror to control the incident direction of the spot and then make the spot centered, and the accuracy of the fast deflector mirror is 2 μrad .

First, the angle of the fast deflector is adjusted to move the center of mass of the light spot to $(-6.4mm,0)$, i.e., $((5w+3d),0)$, and the current value of the detection unit in the second row and the second column is recorded to be set as the threshold value. And the precision and deflection angle of the fast deflector mirror are known, and its deflection angle can be taken as the actual position of the light spot.

4.2.1. Coarse centering test validation. The fast deflector was allowed to move over a range of ±37.15 at 0.5mrad spacing and the angle of deflection was recorded at each moment. Threshold judgment was performed at each point and centered according to the coarse centering algorithm, and the spot position after centering was recorded. The experimental results of the coarse centering algorithm are shown in Fig. 6, with the horizontal coordinate X representing the detected spot position and the Y-axis representing the coordinate position after coarse centering. The shifted spots are all within the range of ±8.50mrad, and the trend is also the same as the simulation results.

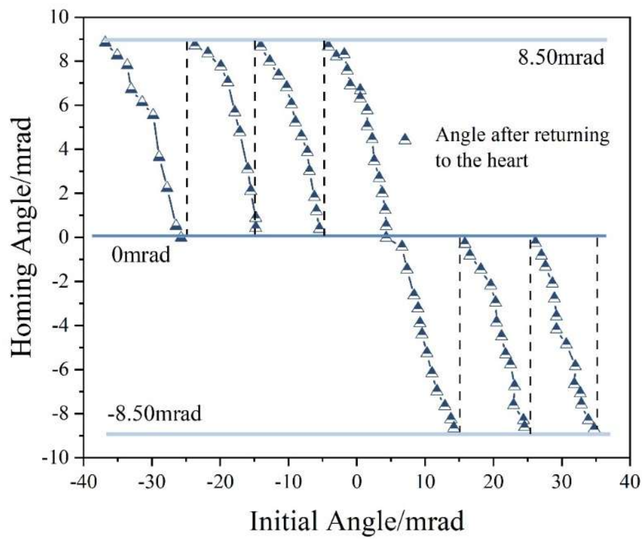

Fig. 6. The results of the results of the crude regression algorithm

4.2.2. Experimental Validation of Algorithms for Precision Centering. The fine homing algorithm uses a database query method, where the spot is first adjusted within ±9.25mrad. A spot was selected every 0.78mrad to determine the solution value 1_{min} and establish the data relationship between each spot angle and the settlement value 1_{min}. Next, let the spot center within the range of ±9.05mrad, every 0.003mrad according to the fine centering algorithm for centering, after centering to adjust the spot size of D_{min}.

The spot position after fine centering is shown in Fig. 7, because the database query method is used, which is divided into 26 intervals, and the results of each interval are similar, so only the results of the spot position in the range of 9.25mrad to 9.98mrad are given in the figure. The horizontal coordinate represents the angle of the light spot after coarse centering, and the vertical coordinate represents the angle after fine centering, and the experimental results show that the light spots after fine centering are all within the range of ±0.78mrad, and the change trend is consistent with the simulation results, so the laser spot position detection algorithm proposed in this paper has the feasibility in fine-tracking light spot position detection.

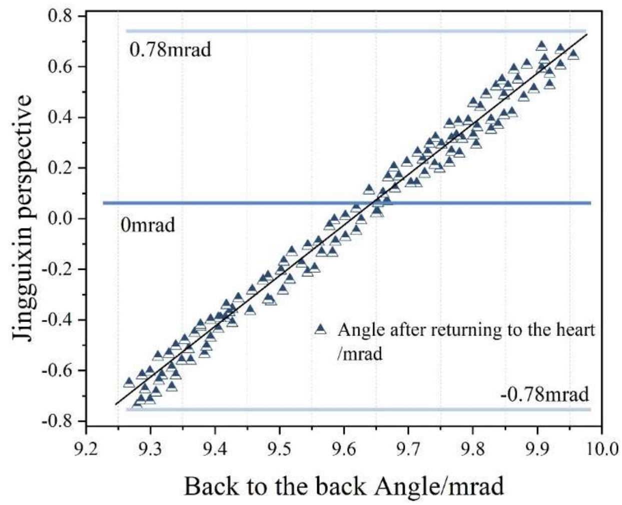

Fig. 7. The location of the light spot after the return of the essence

4.3. Experimental validation of the integration of roughness and precision tracking

The integration of coarse and fine tracking is verified on a testbed for verifying coarse normalization. The feasibility of coarse and fine tracking integration was first verified by combining the edge threshold judgment centering algorithm and the polynomial infinite integration algorithm. The spot was adjusted to a range of ±37.15 angles and moved at 0.5mrad spacing. At each test point, the polynomial infinite integral method was used to track after centering using the edge threshold judgment centering algorithm, and the centered spot position was obtained. The coarse and fine tracking integration errors are shown in Fig. 8. The horizontal coordinate x_0 represents the true position of the light spot, and the vertical coordinate represents the position after centering. From the figure, it can be seen that the difference between the position of the spot after centering and the origin is within 18.5 μrad , which meets the experimental requirements of laser spot position detection.

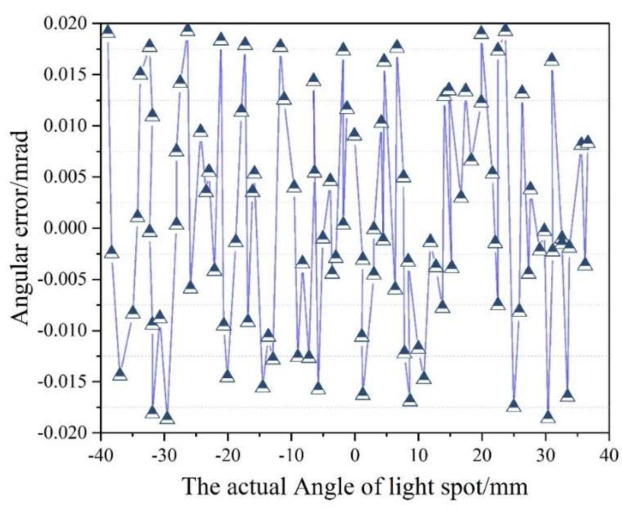

Fig. 8. Coarse, precision tracking integration error

5. Conclusion

In this paper, we propose a laser spot detection method based on CCD image sensor, which adopts the gray scale histogram method to obtain the beacon light, and performs image extraction on the beacon light to get the spot position. The laser spot detection environment is set up, and the laser spot is verified by fine-tracking spot position detection and coarse-tracking spot position detection respectively.

According to the fine-tracking detection spot image processing unit board, simulate its workflow to get the spot off-target amount when the fine-tracking system is not activated, and the amplitude of the coarse-tracking residual sequence is controlled at [-45,35]. The time-domain curve of the fine tracking residuals is densely distributed in [-0.05,0.05], and the histogram data of the fine tracking residuals are mainly distributed in [-0.2,0.2], and the tracking accuracy $\pm 3\mu rad$ is realized.

Controlling the laser output on the coarse tracking test platform, the fast deflector mirror was kept moving in the range of ±37.15 with 0.5mrad spacing in the coarse centering test, and the spot after the coarse movement was in the range of ±8.50mrad, and the trend was also the same as that of the simulation results.

Observe the results of the spot position in the range of 9.25mrad to 9.98mrad for the fine centering algorithm test. The spots after fine centering are all within the range of ±0.78mrad, and the trend is consistent with the simulation results. It proves the feasibility of the laser spot position detection algorithm proposed in this paper in fine-tracking spot position detection.

Funding

This work was supported by National Key Research and Development Program of China in 2022 (Grant No. 2022YFB4601100).

References

[1] Li, N. (2023). Current status and development trend of satellite laser communication. International Journal of Information and Communication Sciences, 8(2), 26-32.

[2] Sha, W., Chanteloup, J. C., & Mourou, Gérard. (2022). Ultrafast fiber technologies for compact laser wake field in medical application. Photonics, 9(6).

[3] Liu, R., Wang, Z., Sparks, T., Liou, F., & Newkirk, J. (2017). Aerospace applications of laser additive manufacturing. Laser Additive Manufacturing, 351-371.

[4] Ji, Q., Zong, S., & Yang, J. (2020). Application and development trend of laser technology in military field. ICOSM 2020: Optoelectronic Science and Materials, 11606.

[5] Zhao, S. (2019). An improved method for spot position detection of a laser tracking and positioning system based on a four-quadrant detector. Sensors, 19.

[6] Lim, H., & Shimizu, Y. (2023). Feasible resolution of angular displacement measurement by an optical angle sensor based on laser autocollimation. Nanomanufacturing and Metrology, 6(1).

[7] Yu, S., & Zhang, J. (2023). Bridge displacement measurement using the gan-network-based spot removal algorithm and the sr-based coarse-to-fine target location method. Structural Control & Health Monitoring.

[8] Hou, S., Lang, X., & Welsher, K. (2017). Robust real-time 3D single-particle tracking using a dynamically moving laser spot. Optics Letters, 42(12), 2390.

[9] Zygmunt, M., & Kopczynski, K. (2020, February). Laser warning system as an element of optoelectronic battlefield surveillance. In Radioelectronic Systems Conference 2019 (Vol. 11442, p. 1144202). SPIE.

[10] Bezpalko, S. O., Shymkovysh, V. M., Kravets, P. I., Novatskyi, A. O., Shymkovysh, L. L., & Doroshenko, A. Y. (2023). Software system for laser targeting dropped ammunition. PROBLEMS IN PROGRAMMING, (2), 10-23.

[11] Wu, Q. L., Zhao, Y., Zhang, Y. N., & Yang, Y. (2021). Characteristics of a new multi-channel sensing device based on C-type photonic crystal fibers. Optics Laser Technology, 134, 106622.

[12] Al Mamun, A., Bappy, M. M., Mudiyanselage, A. S., Li, J., Jiang, Z., Tian, Z., ... & Tian, W. (2023). Multi-channel sensor fusion for real-time bearing fault diagnosis by frequency-domain multilinear principal component analysis. The International Journal of Advanced Manufacturing Technology, 124(3-4), 1321-1334.

[13] Mazumder, O., & Kundu, A. S. (2017). Multi-channel Fusion Based Adaptive Gait Trajectory Generation Using Wearable Sensors. Journal of intelligent & robotic systems: Theory & applications, 86(3), 335-351.

[14] Zeng, Y., Liu, R., & Liu, X. (2021). A novel approach to tool condition monitoring based on multi-sensor data fusion imaging and an attention mechanism. Measurement Science and Technology, 32(5).

[15] Wang, X., Li, K., & Chehri, A. (2024). Multi-Sensor Fusion Technology for 3D Object Detection in Autonomous Driving: A Review. IEEE Transactions on Intelligent Transportation Systems, 25(2).

[16] Zhijie, X., Ye, F., Dai, M., & Zhang, Z. (2021). Real-time fault detection and process control based on multi-channel sensor data fusion. The International Journal of Advanced Manufacturing Technology, 115(3), 795-806.

[17] Qiu, S., Zhao, H., Jiang, N., Wang, Z., Liu, L., An, Y., ... & Fortino, G. (2022). Multi-sensor information fusion based on machine learning for real applications in human activity recognition: State-of-the-art and research challenges. INFORMATION FUSION, 80, 241-265.

[18] Tong, Y., Bai, J., & Chen, X. (2020, October). Research on Multi-sensor Data Fusion Technology. In Journal of Physics: Conference Series (Vol. 1624, No. 3). IOP Publishing.

[19] Xu, X., Tao, Z., Ming, W., An, Q., & Chen, M. (2020). Intelligent monitoring and diagnostics using a novel integrated model based on deep learning and multi-sensor feature fusion. Measurement, 165, 108086.

[20] Lee, G. H., Kwon, K. H., & Kim, M. Y. (2019, July). Ambient Environment Recognition Algorithm Fusing Vision and LiDAR Sensors for Robust Multi-channel V2X System. In 11th International Conference on Ubiquitous and Future Networks, ICUFN 2019 (pp. 98-101). IEEE Computer Society.

[21] Han, J., Cui, L., & Shi, S. (2022). Road rut detection system with embedded multi-channel laser sensor. The International Journal of Advanced Manufacturing Technology, 122(1), 41-50.

[22] Cai, W., Wang, J., Jiang, P., Cao, L., Mi, G., & Zhou, Q. (2020). Application of sensing techniques and artificial intelligence-based methods to laser welding real-time monitoring: A critical review of recent literature. Journal of Manufacturing Systems, 57, 1-18.

[23] Deng Yunkun,Chen Yingping,Huang Jisheng,Wang Ke,Zhao Xianping,Gao Shuyu... & Cheng Yong. (2020). Visualization of Arc Energy Distribution Based on CCD Image Sensor. IOP Conference Series: Earth and Environmental Science(1),012029-.

[24] Lu Chen & Xiong Zilan. (2022). Operation mode recognition of surface microdischarge based on the gray level histogram. Plasma Processes and Polymers(5).

[25] Kishan Shivhare & Gaurav Bhardwaj. (2016). A review on reconfigurable processor for binary image processing. International journal of advanced research (IJAR)(6).